

# iMatching: Imperative Correspondence Learning

Zitong Zhan<sup>1\*</sup>, Dasong Gao<sup>2\*</sup>, Yun-Jou Lin<sup>3</sup>, Youjie Xia<sup>3</sup>, Chen Wang<sup>1†</sup>  
<sup>1</sup>SAIR Lab, IAD, CSE, University at Buffalo, <sup>2</sup>MIT, <sup>3</sup>InnoPeak Technology

{zitongz, chenw}@sairlab.org, dasongg@mit.edu, {rose.lin, youjie.xia}@oppo.com

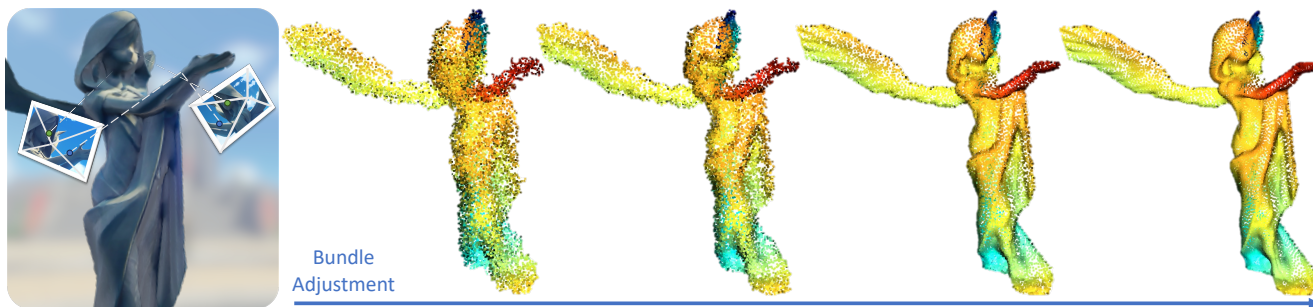


Figure 1. iMatching learns feature correspondence from a bundle adjustment (right), eliminating the need of any ground truth label. Bundle adjustment finds the best landmark position and camera pose and can be used as self-supervision signal for feature correspondence networks.

## Abstract

*Learning feature correspondence is a foundational task in computer vision, holding immense importance for downstream applications such as visual odometry and 3D reconstruction. Despite recent progress in data-driven models, feature correspondence learning is still limited by the lack of accurate per-pixel correspondence labels. To overcome this difficulty, we introduce a new self-supervised scheme, imperative learning (IL), for training feature correspondence. It enables correspondence learning on arbitrary uninterrupted videos without any camera pose or depth labels, heralding a new era for self-supervised correspondence learning. Specifically, we formulated the problem of correspondence learning as a bilevel optimization, which takes the reprojection error from bundle adjustment as a supervisory signal for the model. To avoid large memory and computation overhead, we leverage the stationary point to effectively back-propagate the implicit gradients through bundle adjustment. Through extensive experiments, we demonstrate superior performance on tasks including feature matching and pose estimation, in which we obtained an average of 30% accuracy gain over the state-of-the-art matching models. The source code will be made public to benefit the community.*

## 1. Introduction

Feature correspondence has long been recognized as a pivotal task in computer vision, acting as a cornerstone for

many critical downstream applications such as visual odometry [35], 3D reconstruction [27], and object identification [11]. The essence of accurately matching features across diverse images and viewpoints is invaluable in constructing coherent and precise representations of the visual world.

While recent years have witnessed significant advancements in data-driven models, the task remains intrinsically challenging [1, 21, 28], predominantly due to the absence of sufficient pixel-level annotated data for point matching. Unlike the labels for other computer vision tasks such as object detection where ground truth annotations can be drawn by hand, annotating feature correspondence for every pixel is almost impossible. This constraint has inadvertently limited the potential and generalization ability of the state-of-the-art data-driven models [18, 24]. Moreover, the domain gap in visual appearances between training and testing data also greatly discounted model performance [13].

To alleviate the data problem, there are three common ways. The first way is to simulate correspondence annotation, either from homography transformation [3] or synthetic environments [33]. However, this method often falls short in capturing real-world variations like changes in lighting and occlusions, leading to the sim-to-real gap. The second way is to leverage physical sensors to capture ground truth such as camera pose or depth information. However, this requires specialized equipment like high-end motion capture systems, usually only available indoors and infeasible for outdoor scenes or unique settings like underground environments [40]. Moreover, sensors such as depth cameras and LiDAR tend to offer inaccurate and incomplete depth measurements

\*Equal contribution.

†Corresponding author.

[16], which are inadequate for pixel-level matching [24].

A third way to address the challenge of obtaining large, diverse, and accurately labeled image correspondence datasets has been weakly- and self-supervised methodologies. For example, SGP [37] proposes a student-teacher framework for training the CAPS correspondence model [32] in a self-supervised manner. In SGP, the teacher (RANSAC) and the student model are updated alternately, allowing the teacher to produce pseudo-pose labels for the student model. Nonetheless, this design is limited to models like CAPS, which uses epipolar- instead of reprojection-based loss during training. Moreover, the teacher and student model training is isolated, leading to potential error propagation, *i.e.*, mistakes made by the teacher model can be propagated to the student model, potentially amplifying the issues.

To fully address the data problem, we explore the third category and propose a new self-supervised end-to-end learning framework, iMatching (Figure 1), for feature correspondence using an emerging technique, imperative learning [6, 36]. For the first time, we formulate the problem of feature matching as a bilevel optimization [9] where we direct the learning of the model parameters with an optimization procedure, *i.e.*, bundle adjustment (BA), which is itself an optimization process. Specifically, at the lower level (BA), we optimize the camera pose and the 3D landmark locations that best explain the model-predicted correspondences, whereas, at the higher level (gradient descent), we optimize the network parameters such that the correspondence prediction results in more consistent poses and landmark locations.

Our new formulation for feature correspondence based on bilevel optimization brings distinctive benefits: The low-level optimization eliminates the need for ground truth geometric labels, thanks to the self-correction mechanism brought by bundle adjustment. Such a design can be generalized to any up-to-date matching model. In the experiments, we show that our method is plug-and-play and significantly boosts the performance of state-of-the-art (SOTA) models [1, 5, 14, 28] by an average of 30% and a maximum 82% on pixel-level feature matching on unseen, image-only datasets.

One of the challenges of our formulation is model training which requires differentiating the network through low-level optimization (BA). A popular solution is to backpropagate the errors through the unrolled iterative optimization [8, 30], which is extremely resource-demanding as the temporary variables generated during each iteration need to be stored and traversed for gradient calculation. Instead, we specially designed our loss function so that we can bypass the iterative process during backward pass while still obtaining the gradient. This allowed us to employ a black-box, non-differentiable bundle adjustment to ensure the robustness of training while learning end-to-end *as if* it were differentiable. This end-to-end learnable design also enables the possibility of performing online learning. In summary, our

contributions are summarized as follows:

- We propose the first imperative learning (IL)-based framework for training feature correspondence models with *uninterrupted videos* without any labels such as pose or depth.
- We design an efficient method for propagating the gradient through the bundle adjustment so that we can solve the optimization without differentiating individual steps of the optimization, making end-to-end training possible.
- Through extensive experiments and evaluation on a variety of tasks, we show the superiority of the proposed framework by boosting the performance of the SOTA feature-matching model by 30% precision on the pose estimation task and 13.6% on the feature matching task.

## 2. Related Work

Data-driven methods for feature matching categorized as supervised, weakly- or self-supervised will be introduced in Sec. 2.1 and 2.2, respectively. Additionally, we summarize imperative learning and data-driven models involving bundle adjustment in Sec. 2.3 and 2.4, respectively.

### 2.1. Supervised Methods

Supervised methods rely on known per-pixel correspondences obtained either from (1) synthetic data or (2) indirect ground truth such as depth images and camera poses collected from physical sensors. The first category uses photo-realistic renderers [33] or data augmentation techniques to generate training images. For example, LIFT [38] learns from image samples capturing the same view but with strong illumination change. SuperPoint [3] relies on generic image datasets with homographic transformations. However, those synthetic data techniques may not generalize well to the real-world scenario. For example, homographic transformations can only model scenes where all the points are coplanar.

Most of the existing methods [1, 4, 5, 19, 21, 28, 31] belong to the second category, which leverage collected ground truth depth scan and camera pose data from physical sensors such as motion capture system (MoCap), depth camera, or LiDAR. However, MoCap is confined to dedicated working zones. Scenes like underground urban sewer systems or mines [10] are unable to accommodate complex MoCap devices; depth cameras are limited to indoor environments [16] and provide limited precision, and LiDAR sensors can only provide sparse points. As a result, 3D scene data have a significantly smaller scale compared with generic 2D image due to the complexity of data collection. 3D real world datasets choices are limited. There are only a few datasets such as MegaDepth [15] and ScanNet [2] available for feature correspondence learning, but those datasets are limited to small-scale environments or lack data diversity [24].

### 2.2. Weakly- and Self-supervised Methods

To address the challenges of obtaining large, diverse image datasets with accurate correspondence labels, several efforts

have focused on weakly-supervised methodologies. For instance, CAPS [32] and Patch2Pix [41] eliminate the need for depth information and depend solely on relative camera poses. They leverage the differentiability of matchers by penalizing both epipolar distance and cycle inconsistency.

To further remove the dependency on camera poses, SGP [37] introduced a self-supervised method for training epipolar geometry-based models like CAPS [32] using the teacher-student framework. It introduces RANSAC pose estimation as a teacher to generate pseudo labels for training the student CAPS model. However, the student and teacher training are isolated, which may lead to potential error propagation. Different from SGP, our proposed self-supervised learning framework formulated as bilevel optimization is end-to-end and workable for all models that are directly supervised by pixel locations. This self-supervised dense learning framework can be applied to a wide variety of models as demonstrated in the experiments.

### 2.3. Imperative Learning

Imperative learning (IL) is an emerging self-supervised learning framework based on bilevel optimization. It has been used to tackle problems where both data-driven models and geometry problems are involved. For example, iPlanner [36] adopted a B-spline interpolation [39] as the low-level optimization to guide the network to generate smoothed trajectories for path planning; whereas iSLAM [6] utilized the pose graph optimization to achieve the reciprocal learning for the front-end and back-end in a simultaneous location and mapping (SLAM) system. To the best of our knowledge, IL has not been applied to the problem of feature correspondence learning, and iMatching is the first method for self-supervised feature matching using bundle adjustment.

### 2.4. Bundle Adjustment in Deep Learning

Bundle adjustment (BA) is an optimization technique used in computer vision and photogrammetry to simultaneously estimate the 3D coordinates of landmarks and camera parameters by minimizing the reprojection errors between observed and predicted image points. Recently, several works have tried to integrate BA as part of a neural network. For example, DROID-SLAM [30] uses BA to correct single-view depth estimation during inference so that it is consistent with the geometry shape. For training dense depth and camera poses, BA can be used to encourage geometric consistency between pose and depth prediction [26]. However, to make the BA process differentiable, existing methods [8, 26, 30] unroll the entire iterative second-order optimization process as part of the auto-differentiation graph. This incurs a significant computation and memory overhead since the computation graphs of each iteration need to be kept in memory and traversed during backpropagation. In contrast, we leverage the stationary point of BA, resulting in an extremely efficient one-step implicit gradient computation. As an additional

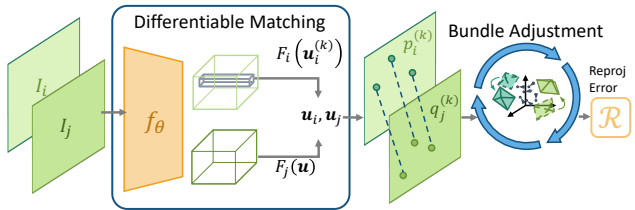


Figure 2. The iMatching framework for feature correspondence learning consists of a feature correspondence network and a bundle adjustment process, which results in a bilevel optimization.

benefit, such a formulation allows us to freely leverage non-differentiable techniques such as alternating pruning and refinement (Sec. 3.1.2) to enhance the robustness of BA.

## 3. Imperative Correspondence Learning

We present an overview of iMatching training scheme and its formulation in Sec. 3.1. The matching network and design of BA are presented in Sec. 3.1.1 and 3.1.2, respectively.

### 3.1. Problem Formulation

The architecture of our iMatching training scheme is shown in Figure 2, which can be divided into two parts, a feature correspondence network  $f_\theta$  parameterized by  $\theta$  and a BA optimization process represented by (1b). The system is formulated as a bilevel optimization problem, expressed as:

$$\min_{\theta} \mathcal{R}(f_\theta; \mathbf{T}^*, \mathbf{p}^*), \quad (1a)$$

$$\text{s. t. } \mathbf{T}^*, \mathbf{p}^* = \underset{\mathbf{T}, \mathbf{p}}{\operatorname{argmin}} \mathcal{R}(\mathbf{T}, \mathbf{p}; f_\theta), \quad (1b)$$

where  $\mathcal{R}$  is the reprojection error function;  $\mathbf{T}_t \in \mathbb{SE}(3)$  are the camera poses in Lie group representation; and  $\mathbf{p}_i \in \mathbb{R}^3$  are the 3D landmark positions. Intuitively, at the lower level, BA finds *the most likely poses and landmark positions* given feature correspondence inferred using network parameters  $\theta$ ; whereas at the upper level, it optimizes for *the best parameters*  $\theta$  for least reprojection error  $\mathcal{R}$  given the estimated poses and landmark positions from the lower level. This training scheme is named *imperative learning* due to this passive reciprocal optimization between the two levels. Since both levels only involve minimizing the projection error, it eliminates the requirements in any form of ground truth. We next present the details of the correspondence network and BA with the solution to bilevel optimization detailed in Sec. 3.2.

#### 3.1.1. Feature Correspondence

Given image pairs  $(I_i, I_j)$ , the feature correspondence network  $f_\theta$  produces a set of  $K$  point correspondences:

$$f_\theta(I_i, I_j) := \{(\mathbf{u}_i^{(k)}, \mathbf{u}_j^{(k)})\}_{k=1}^K, \quad (2)$$

where  $\mathbf{u}_i^{(k)}$  and  $\mathbf{u}_j^{(k)}$  are the 2D coordinates on image  $I_i$  and  $I_j$ , respectively. In practice, given a batch of  $B$  images, we match each image with its past  $n$  ( $1 < n < B$ ) frames.

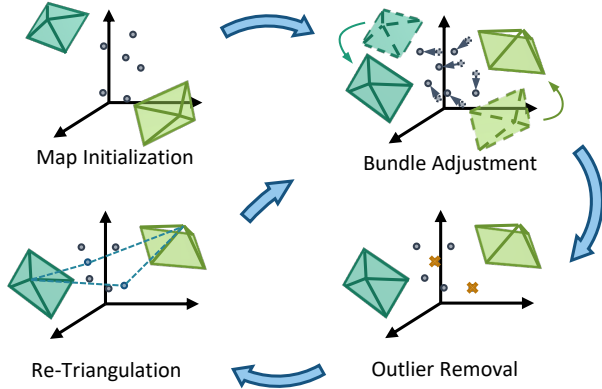


Figure 3. **Iterative bundle adjustment** first initializes the camera poses and landmark positions, and then alternates between optimizing reprojection error and outlier rejection until convergence.

### 3.1.2. Bundle Adjustment

Given a set of correspondences, the BA process seeks to find the optimal pose of the cameras  $\mathbf{T}^* = \{T_i\}_{i=1}^B$  and the 3D positions of landmarks  $\mathbf{p}^* = \{p_l\}_{l=1}^N$  that minimizes the overall reprojection error  $\mathcal{R}$  defined as:

$$\mathcal{R}(\mathbf{T}, \mathbf{p}; f_\theta) = \sum_{j=1}^B \sum_{i=j-n}^{j-1} \sum_{l=1}^P \left\| \mathbf{u}_i^{(k)} - \pi(p_l; T_i) \right\|_2^2, \quad (3)$$

with  $\pi$  being the reprojection function and  $l$  being the index of the point  $p_l$ , which is triangulated from  $\mathbf{u}_i^{(k)}$  and  $\mathbf{u}_j^{(k)}$ .

Next, we describe our design choices that make the BA reliable. As the sole source of supervision, the robustness of BA is fundamental to the success of the training. The BA can be roughly divided into initialization and pruning stages. To obtain an accurate initialization of poses and landmark locations for all frames in the minibatch, we bootstrap the map by localizing and triangulating on a subset of frames before finding the pose of all frames. After all frames are properly initialized, we run a multi-pass BA scheme that alternates between optimization and outlier rejection. We describe each of the steps in the rest of this section.

**Map Initialization** Assume each batched sample  $\{I_t\}_{t=1}^B$  has  $B$  frames from an input sequence. To ensure the robustness and performance of BA, we run structure-from-motion (SfM) on the first  $d$  frames ( $d < B$ ). We first find a frame pair with the most correspondences and parallax as the anchor, and then triangulate the positions of the landmarks within the pair. For other frames, we estimate their transformations with respect to the anchor frames by solving an EPnP [12] on given triangulated 3D positions and 2D correspondences. Lastly, with each frame in the SfM subset having a known camera pose, we triangulate all unused correspondences to obtain the maximum number of landmarks.

**Frame Tracking** For the remaining  $B - d$  frames, we predict their poses sequentially using a constant-velocity

motion model for a rough estimation and then refine the pose estimations by performing a 2D-3D registration against the landmark map generated in the previous step. Existing landmarks observed by those frames are refined by a RANSAC-based multiview triangulation [7].

**Iterative Bundle Adjustment** In this step, we utilize the BA to refine the landmarks and poses estimated above. In practice, single-pass BA is found to be prone to poor convergence due to noise-corrupted keypoint detection and wrong feature correspondences [23, 34]. To solve this challenge, we follow a procedure similar to that of COLMAP [22] that alternates joint optimization and outlier rejection. Specifically, after optimizing the BA objective (1b) with the Levenberg-Marquardt (LM) optimizer, each landmark goes through a filter and re-triangulation process: 3D locations with large reprojection errors are pruned from the set of landmarks at first, and then the surviving ones are updated by re-triangulated landmark locations with the refined camera pose and 2D correspondences. This alternative procedure runs for a small number of iterations. The final poses and landmark positions are used to train the feature correspondence network.

### 3.2. Optimization

To train the network  $f_\theta$  via gradient descent  $\theta \leftarrow \theta - \eta \frac{\partial \mathcal{R}}{\partial \theta}$ , we need to evaluate the derivative of the reprojection error in (1a) w.r.t parameters  $\theta$  of the matching network. According to the chain rule, we can calculate the derivative  $\frac{\partial \mathcal{R}}{\partial \theta}$  as

$$\frac{\partial \mathcal{R}}{\partial \theta} = \left( \frac{\partial \mathcal{R}}{\partial \mathbf{T}^*} \frac{\partial \mathbf{T}^*}{\partial f_\theta} + \frac{\partial \mathcal{R}}{\partial \mathbf{p}^*} \frac{\partial \mathbf{p}^*}{\partial f_\theta} + \frac{\partial \mathcal{R}}{\partial f_\theta} \right) \frac{\partial f_\theta}{\partial \theta}. \quad (4)$$

However, Equation (4) is well defined only if two conditions are satisfied: (1) the matching network  $f_\theta$  is differentiable, *i.e.*,  $\frac{\partial f_\theta}{\partial \theta}$  exists; and (2) the BA in the low-level optimization (1b) is differentiable, *i.e.*,  $\frac{\partial \mathbf{T}^*}{\partial f_\theta}$  and  $\frac{\partial \mathbf{p}^*}{\partial f_\theta}$  exist. However, the challenges of satisfying the two conditions are (1) feature matching is normally represented by matching of discrete pixel locations, while differentiating through the integer pixel locations is unstraightforward; (2) solving the bundle adjustment requires iterative, 2<sup>nd</sup>-order optimizers like LM, which computes large Jacobian matrices and its inversion. This already computationally heavy process makes back-propagating through it difficult. We next describe our solutions to resolve the two challenges.

#### 3.2.1. Differentiable Image Correspondences

A feature correspondence model  $f_\theta$  typically consists of three stages: keypoint detection (optional), feature extraction, and matching prediction [14]. Feature descriptors are generally derived from feature maps  $F_i$  produced by standard backbone networks, through interpolation at the locations of keypoints. The process of matching prediction involves determining the target feature locations based on extracted descriptors. To make the predicted correspondences differentiable, current methods typically compute the feature locations by expectation [32, 41] or regression [1, 5].

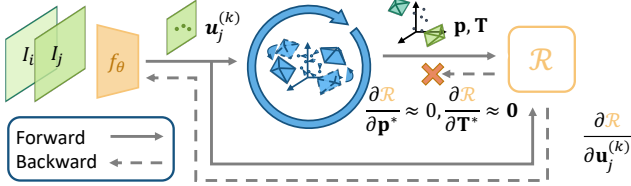


Figure 4. **Gradient flow in iMatching.** During training, the gradient from the reprojection and epipolar losses is only backpropagated through the 2D feature correspondences  $\mathbf{u}_j^{(k)}$  to train the feature matching network. According to our analysis, backpropagation through the robust iterative estimation could be avoided due to the stationarity of optimization outputs  $\mathbf{p}$  and  $\mathbf{T}$ .

**Expectation-based Matching Prediction** Given a feature coordinate  $\mathbf{u}_i^{(k)}$  from  $I_i$  and feature maps  $F_i, F_j$ , the matching coordinate on image  $j$  is an expectation over all possible target feature locations weighted by feature similarity

$$\mathbf{u}_j^{(k)} = \frac{1}{HW} \sum_{\mathbf{u}^{(l)} \in I_j} \mathbf{u}^{(l)} \cdot S\left(F_i(\mathbf{u}_i^{(k)}), F_j(\mathbf{u}^{(l)})\right), \quad (5)$$

where  $S$  can be cosine similarity as an example.

**Regression-based Matching Prediction** As a more generalized version of expectation-based prediction, techniques in this category directly regress the amount of feature shift from the feature maps  $F_i$  and  $F_j$ , using a neural network:

$$\mathbf{u}_j^{(k)} = g_{\theta'}\left(F_i, F_j; \mathbf{u}_i^{(k)}\right), \quad (6)$$

where  $g_{\theta'}$  can be a transformer [1] or a CNN [5]. It is worth noting that iMatching can be used for both categories.

However, there are two non-differentiable cases. First, some keypoint detection networks like SuperPoint [3] have a ranking process with a discrete nature: feature points  $\{\mathbf{u}_i^{(k)}\}_{k=1}^K$  are typically picked from the pixel coordinates with top  $K$  confidence scores. To handle such cases, we can either replace the detection network by a differentiable one or freeze its parameters and thus need not propagate the gradient through it. Second, some methods like [3, 21] use search-based matching prediction. This is completely non-differentiable and is out of the scope of our discussion.

### 3.2.2. Differentiable Bundle Adjustment

An existing widely-used approach to have a differentiable bundle adjustment is to unroll the optimization loop for a fixed number of steps and treat them as part of the forward pass, as done by [8, 29, 30]. However, such a strategy requires the retention of each iteration’s computation graph and the ability to compute the higher-order gradient, which makes this method inapplicable to large-scale problems.

To avoid explicitly computing  $\frac{\partial \mathbf{T}^*}{\partial f_{\theta}}$  and  $\frac{\partial \mathbf{p}^*}{\partial f_{\theta}}$  by differentiating through the iterative optimization process, we leverage

optimization of BA at convergence, which allows us to efficiently backpropagate gradient through the lower level optimization without compromising its robustness. Concretely, since the optimization of BA is unconstrained, at its stationary point (either locally or globally), we have  $\frac{\partial \mathcal{R}}{\partial \mathbf{T}^*} \approx \mathbf{0}$ ,  $\frac{\partial \mathcal{R}}{\partial \mathbf{p}^*} \approx \mathbf{0}$ . Then the gradient (4) becomes

$$\frac{\partial \mathcal{R}}{\partial \theta} = \frac{\partial \mathcal{R}}{\partial f_{\theta}} \frac{\partial f_{\theta}}{\partial \theta}. \quad (7)$$

This implies that to obtain the gradient descent update (1b), it is sufficient to evaluate the reprojection error *only once* after bundle adjustment and back-propagate through the correspondence argument, treating  $\mathbf{T}^*$  and  $\mathbf{p}^*$  as given. Then,  $f_{\theta}$  can be trained with SGD with the gradient given by (7). Figure 4 illustrates such a gradient flow.

It is worth noting that Ji et al. [9, Table 1, N-loop AID] proved that, as long as the upper-level optimization has a properly small step size, the bilevel optimization is guaranteed to converge, even if the lower-level optimization has not converged. Although [9] assumes that the lower-level optimization uses 1<sup>st</sup>-order optimizers like SGD, we empirically found the bilevel optimization can still converge using 2<sup>nd</sup>-order optimizers with just a few iterations.

### 3.2.3. Improving Training Convergence

To further improve the convergence of training, we retain the coarse-to-fine training scheme which is common in feature correspondence models. These models typically first obtain a rough estimate having the same format as in Sec. 3.1.1 from low-resolution image features, and then refine the result using a higher-resolution feature or a cropped image patch to produce fine matching. While the BA in Sec. 3.1.2 is only applied on the fine estimate for the best accuracy, the initial rough estimate receives the same gradient update in (7).

## 4. Experiments

We show the effectiveness of our method by presenting the performance gain after training SOTA correspondence models with iMatching on unseen, *image-only* datasets. We experiment with CAPS [32], Patch2Pix [41], ASpanFormer [1], and DKM [5], and name the models using our iMatching training scheme as iCAPS, iPatch2Pix, iASpan, and iDKM respectively. We also compare with SGP [37], which, to the best of our knowledge, is the only self-supervised method.

### 4.1. Datasets

**TartanAir** [33] is a large (3TB) and diverse synthetic SLAM dataset. Collected in photo-realistic simulation environments, the dataset contains precise ground truth depth and pose labels and covers a wide range of scene types as well as challenging conditions such as dynamic lighting and adverse weather. We use TartanAir to evaluate pixel-level matching accuracy since it is synthesized and thus free of sensor noises. We exclude scenes where ground truth matching is unavailable, e.g., textureless areas or fast moving dynamic objects.

Scene	Indoor			Outdoor			Natural			Artificial			Mixed			Easy			Hard			Overall		
	1px	2px	5px	1px	2px	5px	1px	2px	5px	1px	2px	5px	1px	2px	5px	1px	2px	5px	1px	2px	5px	1px	2px	5px
(a) Non-differentiable Matcher																								
SIFT	22.6	31.7	41.9	22.9	31.0	38.3	16.0	23.2	30.5	24.9	33.8	42.7	24.1	32.5	39.7	23.7	32.5	40.8	21.4	29.4	37.4	22.8	31.2	39.3
ORB	20.8	40.2	58.5	16.5	32.0	45.9	10.2	21.2	33.0	20.1	38.4	55.0	18.5	35.9	50.9	18.8	36.5	52.1	16.7	32.4	47.2	17.7	34.4	49.6
SuperGlue	39.6	64.2	85.0	38.2	62.4	80.9	27.2	49.0	71.0	41.9	66.8	85.6	40.4	65.4	83.2	40.7	65.8	84.1	36.7	60.2	80.2	38.6	62.9	82.1
R2D2	30.6	48.6	64.8	31.4	48.6	61.0	25.2	41.4	55.1	32.9	50.5	64.7	32.0	50.1	62.4	32.3	50.6	64.3	29.1	45.7	59.6	31.1	48.6	62.2
(b) Pretrained Models of End-to-end Differentiable Matcher (Supervised)																								
CAPS	26.6	62.3	87.3	27.1	63.3	87.3	21.1	52.7	81.0	28.0	64.6	88.1	29.0	67.1	90.0	28.4	66.2	89.4	25.5	60.1	85.3	26.9	63.0	87.3
Patch2Pix	0.7	3.5	23.6	0.9	4.6	25.8	1.0	4.9	26.1	0.8	4.1	24.9	0.8	4.3	25.0	0.9	4.6	26.6	0.8	4.0	23.9	0.8	4.3	25.2
ASpanFormer	51.5	76.9	94.2	51.5	76.7	93.3	43.7	70.1	90.6	52.2	77.8	94.3	55.4	79.3	94.2	55.8	80.9	95.2	47.4	72.9	92.0	51.5	76.8	93.6
(c) Self-supervised Baseline																								
SGP	44.8	70.5	88.7	47.7	71.8	88.7	36.6	60.7	83.1	47.5	72.6	89.2	52.5	76.5	91.6	50.8	75.5	90.8	43.1	67.6	86.7	46.8	71.4	88.7
(d) Models Using Our iMatching Training Scheme (Self-supervised)																								
iCAPS (Ours)	47.5	70.9	88.3	49.7	72.9	89.7	40.4	63.8	85.6	50.1	73.3	89.4	53.0	76.3	91.5	53.0	76.0	91.0	45.3	68.9	87.7	49.0	72.3	89.3
iPatch2Pix (Ours)	6.1	17.3	42.1	7.5	20.6	44.5	7.3	20.2	43.8	5.8	17.4	42.5	9.3	23.4	46.3	8.3	22.9	49.0	6.0	16.7	39.0	7.1	19.7	43.8
iASpan (Ours)	<b>60.1</b>	<b>79.0</b>	<b>95.0</b>	<b>57.8</b>	<b>78.7</b>	<b>94.2</b>	<b>51.7</b>	<b>73.6</b>	<b>91.8</b>	<b>58.6</b>	<b>78.9</b>	<b>95.1</b>	<b>62.7</b>	<b>82.0</b>	<b>94.9</b>	<b>63.1</b>	<b>82.9</b>	<b>96.0</b>	<b>54.0</b>	<b>74.9</b>	<b>92.9</b>	<b>58.4</b>	<b>78.8</b>	<b>94.4</b>

Table 1. Mean matching accuracy (%) on the TartanAir dataset under error tolerance of 1, 2, and 5 pixels. Our iMatching training scheme consistently boosts the accuracy of feature matching models, with finetuned results shown in “iCAPS”, “iPatch2Pix”, and “iASpan”.

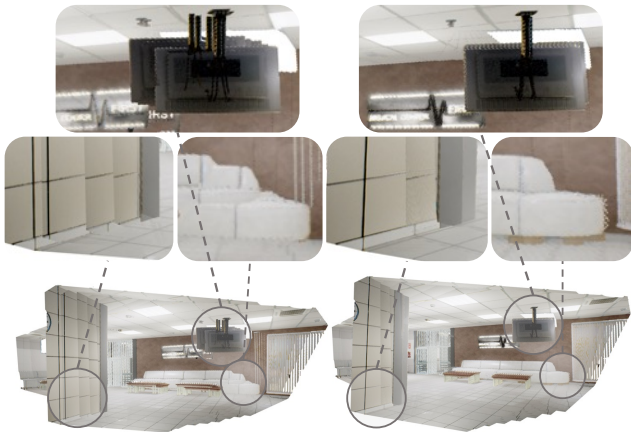


Figure 5. Pose estimation comparison between pretrained and finetuned model. The bottom point clouds are reconstructed by aligning RGBD scans using RANSAC-estimated poses derived from feature correspondence. The pretrained CAPS model (left) creates artifacts on the sofa and monitor due to inaccurately estimated poses and falsely aligned depth map, while such artifacts are not presented in the finetuned model (right). Best viewed digitally.

We divide each valid scene into subsets of size 8.5:0.5:1 for training, validation, and testing, respectively.

**ETH3D-SLAM** [25] provides RGBD sequences captured in the real world. Its scenes primarily consist of small-scale objects with complex details. We exclude the scenes where RGB camera do not provide information in a completely dark environment or is moved while its view is blocked.

MegaDepth [15] and ScanNet [2] datasets are not employed because they only provide discrete images, while iMatching assumes uninterrupted videos to be available. Moreover, these datasets are not suitable for evaluating feature matching because of a lack of pixel-level accuracy, as their ground truth is generated from structure-from-motion.

## 4.2. Feature Matching

**Evaluation Protocol** For each method, we report the mean matching accuracy (MMA), *i.e.*, the percentage of predicted correspondences with reprojection errors less than 1, 2, and 5 pixels. The ground truth correspondences are computed based on the TartanAir’s pose and depth map.

**Baselines** We compare against most of the widely used and state-of-the-art models. We divide them into three categories: (a) non-differentiable models including SIFT [17], ORB [20], SuperGlue [21], and R2D2 [19], (b) the state-of-the-art models including CAPS [32], Patch2Pix [41], and ASpanFormer [1], and (c) self-supervised method, SGP [37]. SGP is specifically designed for CAPS [32]. For fairness, both SGP and our iMatching are initialized with the exact same pretrained weights as provided by [32].

**Results** We report the MMA of selected methods in Table 1. It can be seen that methods trained with iMatching greatly outperform previous handcrafted, supervised, and self-supervised methods. Comparing categories (a) and (b), we demonstrate that self-supervision can further enhance data-driven methods, which already outperform handcrafted features in our zero-shot scenario except for Patch2Pix.

Method	SuperGlue [21]			SGP [37]			CAPS [32]			iCAPS (Ours)				DKM [5]			iDKM (Ours)			
	5°	10°	20°	5°	10°	20°	5°	10°	20°	5°	10°	20°	% ↑	5°	10°	20°	5°	10°	20°	% ↑
cables	66.9	72.6	75.4	62.0	67.9	70.9	67.4	73.9	77.1	<b>69.0</b>	<b>76.3</b>	<b>80.0</b>	2.4%	59.2	63.7	66.0	<b>84.4</b>	<b>91.6</b>	<b>95.2</b>	42.6%
camera_shake	64.5	78.0	86.1	68.4	82.1	89.8	63.0	77.8	87.0	<b>72.3</b>	<b>84.1</b>	<b>90.8</b>	14.8%	65.9	72.9	76.5	<b>67.7</b>	<b>74.2</b>	<b>77.4</b>	2.7%
ceiling	81.0	86.6	89.7	78.9	85.0	88.1	81.4	87.8	91.1	<b>83.9</b>	<b>91.0</b>	<b>94.6</b>	3.1%	59.4	62.8	64.6	<b>76.6</b>	<b>83.8</b>	<b>87.5</b>	29.0%
desk	77.1	84.5	88.4	73.5	82.3	87.0	72.8	82.2	87.3	<b>74.4</b>	<b>83.9</b>	<b>88.9</b>	2.2%	82.8	85.3	86.8	<b>82.9</b>	<b>85.5</b>	<b>86.9</b>	0.1%
desk_changing	71.3	77.2	80.4	69.7	76.8	80.4	73.5	81.6	85.8	<b>74.3</b>	<b>83.1</b>	<b>87.8</b>	1.1%	61.2	62.9	63.7	<b>75.3</b>	<b>86.1</b>	<b>91.8</b>	23.0%
einstein	57.1	62.0	64.8	66.7	72.4	75.8	67.8	74.1	77.8	<b>69.8</b>	<b>76.6</b>	<b>80.5</b>	2.9%	36.6	38.2	39.4	<b>63.4</b>	<b>68.4</b>	<b>71.3</b>	73.2%
einstein_GLC	42.3	46.1	48.4	51.7	57.4	60.7	51.3	56.7	60.3	<b>53.6</b>	<b>59.3</b>	<b>63.0</b>	4.5%	35.5	41.0	45.9	<b>53.1</b>	<b>62.1</b>	<b>69.9</b>	49.6%
mannequin	76.2	80.6	83.0	80.1	84.9	87.5	80.2	85.3	88.0	<b>83.9</b>	<b>89.5</b>	<b>92.5</b>	4.6%	59.5	60.9	61.6	<b>81.1</b>	<b>88.1</b>	<b>91.6</b>	36.3%
mannequin_face	69.1	71.0	71.9	73.2	76.3	77.9	73.4	76.8	78.5	<b>77.2</b>	<b>81.3</b>	<b>83.3</b>	5.2%	53.9	54.3	54.5	<b>71.3</b>	<b>73.7</b>	<b>74.8</b>	32.3%
planar	67.7	78.9	84.5	65.6	79.5	86.7	67.1	81.6	88.9	<b>69.3</b>	<b>83.3</b>	<b>91.0</b>	3.3%	62.9	70.6	74.4	<b>71.3</b>	<b>81.1</b>	<b>86.4</b>	13.4%
plant	78.5	82.2	84.1	74.4	80.2	83.0	71.9	78.5	81.7	<b>81.0</b>	<b>88.0</b>	<b>91.5</b>	12.7%	86.5	88.9	90.0	<b>88.4</b>	<b>91.1</b>	<b>92.4</b>	2.2%
plant_scene	72.6	77.2	79.6	71.0	76.4	79.2	71.8	77.7	80.7	<b>80.2</b>	<b>86.8</b>	<b>90.2</b>	11.7%	44.2	45.2	45.7	<b>83.5</b>	<b>90.7</b>	<b>94.3</b>	88.9%
sfm_lab_room	87.7	93.8	96.9	<b>90.6</b>	<b>95.3</b>	<b>97.6</b>	86.4	93.3	96.6	90.4	95.2	<b>97.6</b>	4.6%	92.0	94.4	95.6	<b>94.2</b>	<b>97.1</b>	<b>98.6</b>	2.4%
sofa	69.2	76.9	81.4	70.8	79.6	84.2	70.8	79.6	84.1	<b>72.2</b>	<b>81.5</b>	<b>86.9</b>	2.0%	52.9	54.2	54.8	<b>80.1</b>	<b>89.1</b>	<b>94.9</b>	51.4%
table	65.3	68.8	70.6	65.3	69.4	71.4	70.5	75.3	77.7	<b>77.4</b>	<b>83.3</b>	<b>86.3</b>	9.8%	28.6	29.4	29.8	<b>78.2</b>	<b>90.0</b>	<b>94.5</b>	173.4%
vicon_light	69.4	76.0	79.6	72.7	81.1	85.6	<b>73.2</b>	<b>82.0</b>	<b>86.6</b>	71.8	81.3	86.4	-1.9%	66.5	70.1	72.1	<b>74.5</b>	<b>80.3</b>	<b>83.3</b>	12.0%
large_loop	69.2	75.1	78.1	69.9	75.8	78.8	73.2	79.3	82.4	<b>78.6</b>	<b>86.2</b>	<b>90.3</b>	7.4%	42.5	45.1	46.4	<b>77.7</b>	<b>86.8</b>	<b>91.5</b>	82.8%
Overall	69.7	75.8	79.0	70.9	77.8	81.4	71.5	79.0	83.0	<b>75.3</b>	<b>83.0</b>	<b>87.1</b>	5.3%	58.2	61.2	62.8	<b>76.7</b>	<b>83.5</b>	<b>87.2</b>	31.8%

Table 2. **Pose Estimation Accuracy on ETH3D-SLAM.** The best results are highlighted in bold. The column “SGP” is the accuracy of the finetuned model of CAPS using the self-supervised SGP training scheme. The columns “CAPS” and “DKM” are the accuracies of the pretrained models from their original works. The columns “iCAPS” and “iDKM” are accuracies of CAPS and DKM trained by our iMatching self-supervised learning, with percentage of improvements under 5° threshold calculated in “%↑”.

Compared with the pretrained supervised methods in (b), iCAPS in (d) offers 1.82× of the accuracy of the pretrained CAPS at 1-pixel error tolerance. Figure 5 compares the CAPS and iCAPS model on simple point cloud registration tasks, with ground truth depth scan used to highlight pose estimation accuracy. The pretrained model leaves obvious misalignments even if BA is used to promote consensus of camera poses, which indicates flaws in both the model accuracy and robustness of a normal BA, but our bilevel optimization successfully eliminates the artifacts. Patch2Pix and ASpanFormer are two models showing weak and strong zero-shot performance, respectively. Our iASpan is capable of improving the already strong ASpanFormer model by 13.6%, and more qualitative results are available in Figure 6. Additionally, we observe a strong performance boost of 8.9× on Patch2Pix, even though it’s a poorly performed model initially. This shows that our bilevel optimization formulation is robust against large numbers of outliers.

In addition, our method outperforms SGP by a 5% higher performance gain, as indicated by (c) and iCAPS in (d). Our method has a relatively obvious advantage on Natural scenes. They contain repeating texture patterns and complex lighting conditions, e.g. the vegetation in the 4<sup>th</sup> sample in Figure 6. These conditions typically cause frequent mismatched correspondence and thus highlight the importance of outlier rejection capability in self-supervised systems. We

conclude that our experiments on CAPS, Patch2Pix, and ASpanFormer show the strong adaptability of iMatching by covering major types of end-to-end differentiable models.

### 4.3. Relative Pose Estimation

We next conduct another task, relative pose estimation, which is a crucial application in computer vision, to demonstrate the adaptability of the iMatching training scheme. We follow [1] to recover the camera pose by solving the essential matrix from the predicted correspondences using RANSAC. **Baselines** To evaluate the performance gain after training, we use both expectation- and regression-based methods with pre-trained weights, as represented by CAPS [32] and DKM [5], respectively. Again, we compare against SGP [37] by training CAPS with iMatching. The non-differentiable SuperGlue model [21] is included for reference.

**Accuracy** A pose estimate is considered to be correct if the angular error in both rotation and translation falls below thresholds of 5°, 10°, and 20°, and we report the area-under-curve (AUC) of the pose error in Table 2. iMatching shows superior performance over supervised and self-supervised methods. Data-driven methods perform strongly, except for the DKM. Despite demonstrating the strongest performance under supervised setting on MegaDepth and ScanNet [5], DKM is behind SuperGlue and CAPS by a large margin on the unseen ETH3D-SLAM scenes. However, iMatching is able to boost its accuracy by 30% compared with

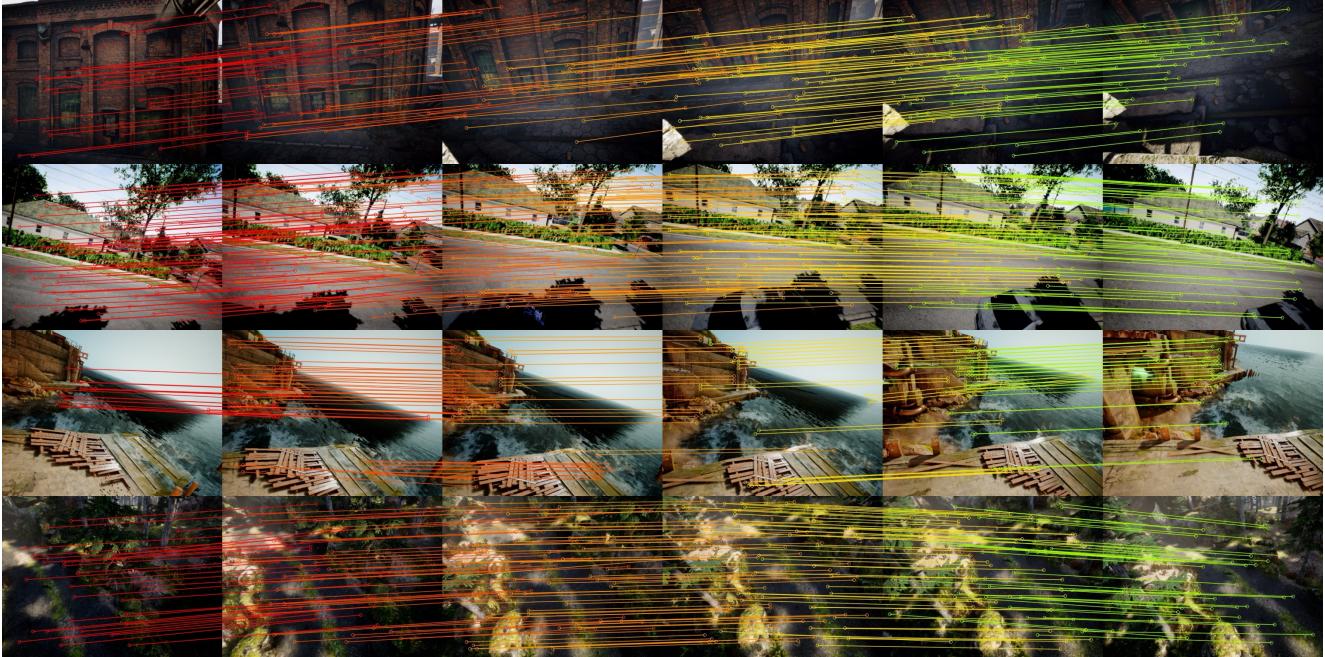


Figure 6. **iASpan Qualitative Results.** Each row shows an uninterrupted video with 10% of the correspondences. Best viewed digitally.

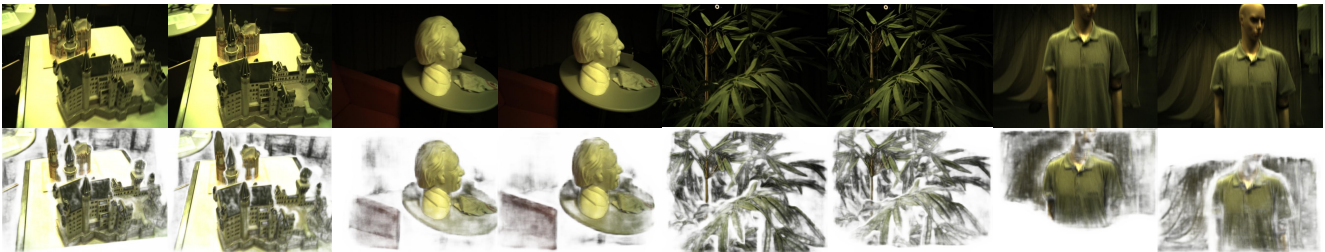


Figure 7. **iDKM Qualitative Results.** The top rows (1, 3) show raw image pairs  $I_i$  and  $I_j$ . These qualitative results contain restored RGB pixel values of one image by transferring pixel color given the estimated feature correspondences from the other image. Our iDKM accurately identifies matching on the features best explained by object shape. Best viewed digitally.

the pretrained, making it the strongest among all methods. From image warping results in Figure 7, it also demonstrates satisfying per-pixel matching quality.

**Comparison with SGP** Pose estimation accuracy improvement brought by SGP is only observed in 5 scenes and is overall negligible. This is primarily because the CAPS model has strong generalizability in the task but the simple supervision formulation in CAPS already has saturated performance under the evaluation metrics: SGP training can only encourage overall consensus between correspondence following the epipolar constraint regardless of actual 3D shape, so the effectiveness of SGP is not as obvious as what we observed in feature matching. In contrast, our design allows us to further improve the already strong CAPS model by 5%. Our iDKM experiment also verifies that iMatching is less likely to be vulnerable to initially worse pose estimation accuracy, as its iterative BA process brings additional robustness to correct error that occurs in map initialization. Therefore, we conclude that our imperative learning works pragmatically

and effectively, thanks to its carefully designed robust BA.

## 5. Conclusion

We explore an exciting new direction in self-supervised feature correspondence learning, *i.e.* imperative learning, using bundle adjustment as a supervision signal, formulated as a bilevel optimization problem, and learning feature correspondence from uninterrupted video sequence without any form of ground truth labels. We highlight the simple and efficient optimization technique used to differentiate through the complex bundle adjustment process. We experimented with the state-of-the-art models and demonstrated obvious performance leaps in tasks including feature matching and relative pose estimation, empirically verifying the importance of our robust bundle adjustment. This paper makes an attractive starting point for integrating the learning process of feature correspondence to downstream applications such as visual odometry and 3D reconstruction in an online manner.



## Acknowledgements

This work was in part supported by the ONR award N00014-24-1-2003. Any opinions, findings, conclusions, or recommendations expressed in this paper are those of the authors and do not necessarily reflect the views of the ONR. The authors wish to express their gratitude for the generous gift funding provided by Cisco Systems Inc. and InnoPeak Technology Inc.

## References

- [1] Hongkai Chen, Zixin Luo, Lei Zhou, Yurun Tian, Mingmin Zhen, Tian Fang, David McKinnon, Yanghai Tsin, and Long Quan. Aspanformer: Detector-free image matching with adaptive span transformer. In *Computer Vision—ECCV 2022: 17th European Conference, Tel Aviv, Israel, October 23–27, 2022, Proceedings, Part XXXII*, pages 20–36. Springer, 2022. 1, 2, 4, 5, 6, 7
- [2] Angela Dai, Angel X Chang, Manolis Savva, Maciej Halber, Thomas Funkhouser, and Matthias Nießner. Scannet: Richly-annotated 3d reconstructions of indoor scenes. In *Proceedings of the IEEE conference on computer vision and pattern recognition*, pages 5828–5839, 2017. 2, 6
- [3] Daniel DeTone, Tomasz Malisiewicz, and Andrew Rabinovich. Superpoint: Self-supervised interest point detection and description. In *Proceedings of the IEEE conference on computer vision and pattern recognition workshops*, pages 224–236, 2018. 1, 2, 5
- [4] Mihai Dusmanu, Ignacio Rocco, Tomas Pajdla, Marc Pollefeys, Josef Sivic, Akihiko Torii, and Torsten Sattler. D2-net: A trainable cnn for joint detection and description of local features. *arXiv preprint arXiv:1905.03561*, 2019. 2
- [5] Johan Edstedt, Ioannis Athanasiadis, Mårten Wadenbäck, and Michael Felsberg. DKM: Dense kernelized feature matching for geometry estimation. In *IEEE Conference on Computer Vision and Pattern Recognition*, 2023. 2, 4, 5, 7
- [6] Taimeng Fu, Shaoshu Su, and Chen Wang. iSLAM: Imperative SLAM. *arXiv preprint arXiv:2306.07894*, 2023. 2, 3
- [7] Richard Hartley and Andrew Zisserman. *Multiple view geometry in computer vision*. Cambridge university press, 2003. 4
- [8] Krishna Murthy Jatavallabhula, Ganesh Iyer, and Liam Paull.  $\nabla$ slam: Dense slam meets automatic differentiation. In *2020 IEEE International Conference on Robotics and Automation (ICRA)*, pages 2130–2137. IEEE, 2020. 2, 3, 5
- [9] Kaiyi Ji, Junjie Yang, and Yingbin Liang. Bilevel optimization: Convergence analysis and enhanced design. In *International conference on machine learning*, pages 4882–4892. PMLR, 2021. 2, 5
- [10] Mike Kasper, Steve McGuire, and Christoffer Heckman. A Benchmark for Visual-Inertial Odometry Systems Employing Onboard Illumination. In *Intelligent Robots and Systems (IROS)*, 2019. 2
- [11] Nikhil Varma Keetha, Chen Wang, Yuheng Qiu, Kuan Xu, and Sebastian Scherer. AirObject: A temporally evolving graph embedding for object identification. In *IEEE/CVF Conference on Computer Vision and Pattern Recognition (CVPR)*, 2022. 1
- [12] Vincent Lepetit, Francesc Moreno-Noguer, and Pascal Fua. Ep n p: An accurate o (n) solution to the p n p problem. *International journal of computer vision*, 81:155–166, 2009. 4
- [13] Shunkai Li, Xin Wang, Yingdian Cao, Fei Xue, Zike Yan, and Hongbin Zha. Self-supervised deep visual odometry with online adaptation. In *Proceedings of the IEEE/CVF Conference on Computer Vision and Pattern Recognition*, pages 6339–6348, 2020. 1
- [14] Xinghui Li, Kai Han, Shuda Li, and Victor Prisacariu. Dual-resolution correspondence networks. *Advances in Neural Information Processing Systems*, 33:17346–17357, 2020. 2, 4
- [15] Zhengqi Li and Noah Snavely. Megadepth: Learning single-view depth prediction from internet photos. In *Proceedings of the IEEE conference on computer vision and pattern recognition*, pages 2041–2050, 2018. 2, 6
- [16] Alexandre Lopes, Roberto Souza, and Helio Pedrini. A survey on rgb-d datasets. *arXiv preprint arXiv:2201.05761*, 2022. 2
- [17] David G. Lowe. Distinctive image features from scale-invariant keypoints. *Int. J. Comput. Vision*, 60(2):91–110, 2004. 6
- [18] Zixin Luo, Tianwei Shen, Lei Zhou, Siyu Zhu, Runze Zhang, Yao Yao, Tian Fang, and Long Quan. Geodesc: Learning local descriptors by integrating geometry constraints. In *Proceedings of the European conference on computer vision (ECCV)*, pages 168–183, 2018. 1
- [19] Jerome Revaud, Philippe Weinzaepfel, César De Souza, Noe Pion, Gabriela Csurka, Yohann Cabon, and Martin Humenberger. R2d2: repeatable and reliable detector and descriptor. *arXiv preprint arXiv:1906.06195*, 2019. 2, 6
- [20] Ethan Rublee, Vincent Rabaud, Kurt Konolige, and Gary R. Bradski. Orb: An efficient alternative to sift or surf. *2011 International Conference on Computer Vision*, pages 2564–2571, 2011. 6
- [21] Paul-Edouard Sarlin, Daniel DeTone, Tomasz Malisiewicz, and Andrew Rabinovich. SuperGlue: Learning feature matching with graph neural networks. In *Proceedings of the IEEE/CVF conference on computer vision and pattern recognition*, pages 4938–4947, 2020. 1, 2, 5, 6, 7
- [22] Johannes Lutz Schönberger and Jan-Michael Frahm. Structure-from-motion revisited. In *Conference on Computer Vision and Pattern Recognition (CVPR)*, 2016. 4
- [23] Johannes Lutz Schönberger, Enliang Zheng, Marc Pollefeys, and Jan-Michael Frahm. Pixelwise view selection for unstructured multi-view stereo. In *European Conference on Computer Vision (ECCV)*, 2016. 4
- [24] Johannes L Schonberger, Hans Hardmeier, Torsten Sattler, and Marc Pollefeys. Comparative evaluation of hand-crafted and learned local features. In *Proceedings of the IEEE conference on computer vision and pattern recognition*, pages 1482–1491, 2017. 1, 2
- [25] Thomas Schöps, Torsten Sattler, and Marc Pollefeys. BAD SLAM: Bundle adjusted direct RGB-D SLAM. In *Conference on Computer Vision and Pattern Recognition (CVPR)*, 2019. 6

- [26] Yunxiao Shi, Jing Zhu, Yi Fang, Kuochin Lien, and Junli Gu. Self-supervised learning of depth and ego-motion with differentiable bundle adjustment. *arXiv preprint arXiv:1909.13163*, 2019. 3
- [27] Elisavet Konstantina Stathopoulou, M Welpöner, and Fabio Remondino. Open-source image-based 3d reconstruction pipelines: Review, comparison and evaluation. *The International Archives of the Photogrammetry, Remote Sensing and Spatial Information Sciences, Volume XLII-2/W17*, pages 331–338, 2019. 1
- [28] Jiaming Sun, Zehong Shen, Yuang Wang, Hujun Bao, and Xiaowei Zhou. Loftr: Detector-free local feature matching with transformers. In *Proceedings of the IEEE/CVF conference on computer vision and pattern recognition*, pages 8922–8931, 2021. 1, 2
- [29] Zachary Teed and Jia Deng. Raft: Recurrent all-pairs field transforms for optical flow. In *European conference on computer vision*, pages 402–419. Springer, 2020. 5
- [30] Zachary Teed and Jia Deng. Droid-slam: Deep visual slam for monocular, stereo, and rgb-d cameras. *Advances in Neural Information Processing Systems*, 34:16558–16569, 2021. 2, 3, 5
- [31] Chen Wang, Yuheng Qiu, Dasong Gao, and Sebastian Scherer. Lifelong graph learning. In *IEEE/CVF Conference on Computer Vision and Pattern Recognition (CVPR)*, 2022. 2
- [32] Qianqian Wang, Xiaowei Zhou, Bharath Hariharan, and Noah Snavely. Learning feature descriptors using camera pose supervision. In *European Conference on Computer Vision*, pages 757–774. Springer, 2020. 2, 3, 4, 5, 6, 7
- [33] Wenshan Wang, DeLong Zhu, Xiangwei Wang, Yaoyu Hu, Yuheng Qiu, Chen Wang, Yafei Hu, Ashish Kapoor, and Sebastian Scherer. Tartanair: A dataset to push the limits of visual slam. In *IEEE/RSJ International Conference on Intelligent Robots and Systems (IROS)*, pages 4909–4916, 2020. 1, 2, 5
- [34] Changchang Wu. Towards linear-time incremental structure from motion. In *2013 International Conference on 3D Vision-3DV 2013*, pages 127–134. IEEE, 2013. 4
- [35] Kuan Xu, Yuefan Hao, Shenghai Yuan, Chen Wang, and Lihua Xie. AirVO: An illumination-robust point-line visual odometry. In *IEEE/RSJ International Conference on Intelligent Robots and Systems (IROS)*, 2023. 1
- [36] Fan Yang, Chen Wang, Cesar Cadena, and Marco Hutter. Iplanner: Imperative path planning. In *Robotics: Science and Systems (RSS)*, 2023. 2, 3
- [37] Heng Yang, Wei Dong, Luca Carlone, and Vladlen Koltun. Self-supervised geometric perception. In *Proceedings of the IEEE/CVF Conference on Computer Vision and Pattern Recognition*, pages 14350–14361, 2021. 2, 3, 5, 6, 7
- [38] Kwang Moo Yi, Eduard Trulls, Vincent Lepetit, and Pascal Fua. Lift: Learned invariant feature transform. In *European conference on computer vision*, pages 467–483. Springer, 2016. 2
- [39] Zitong Zhan, Xiangfu Li, Qihang Li, Haonan He, Abhinav Pandey, Haitao Xiao, Yangmengfei Xu, Xiangyu Chen, Kuan Xu, Kun Cao, Zhipeng Zhao, Zihan Wang, Huan Xu, Zihang Fang, Yutian Chen, Wentao Wang, Xu Fang, Yi Du, Tianhao Wu, Xiao Lin, Yuheng Qiu, Fan Yang, Jingnan Shi, Shaoshu Su, Yiren Lu, Taimeng Fu, Karthik Dantu, Jiajun Wu, Lihua Xie, Marco Hutter, Luca Carlone, Sebastian Scherer, Daning Huang, Yaoyu Hu, Junyi Geng, and Chen Wang. PyPose v0.6: The imperative programming interface for robotics. In *IEEE/RSJ International Conference on Intelligent Robots and Systems (IROS) Workshop*, 2023. 3
- [40] Shibo Zhao, Damanpreet Singh, Haoxiang Sun, Rushan Jiang, YuanJun Gao, Tianhao Wu, Jay Karhade, Chuck Whittaker, Ian Higgins, Jiahe Xu, Yuheng Qiu, Sourojit Saha, Chen Wang, Wenshan Wang, and Sebastian Scherer. Subt-mrs: A subterranean, multi-robot, multi-spectral and multi-degraded dataset for robust slam. *arXiv preprint arXiv:2307.07607*, 2023. 1
- [41] Qunjie Zhou, Torsten Sattler, and Laura Leal-Taixe. Patch2pix: Epipolar-guided pixel-level correspondences. In *Proceedings of the IEEE/CVF conference on computer vision and pattern recognition*, pages 4669–4678, 2021. 3, 4, 5, 6